Parameter errata in flexible myocardial PET protocol compared to conventional fixed ones

BSc Maria Virtanen

MSc thesis
December 2023

Reviewers:
Prof. Riku Klén
PhD Jouni Tuisku

DEPARTMENT OF MATHEMATICS AND STATISTICS

UNIVERSITY OF TURKU
Department of Mathematics and Statistics

VIRTANEN, MARIA: Parameter errata in flexible myocardial PET protocol compared to conventional fixed ones
MSc Thesis, 27 pages, 8 appendix pages
Applied mathematics
December 2023

This MSc thesis is studying flexible myocardial radiowater PET protocols. The compartment model giving the parameters is presented, and mathematical concepts like the Laplace transform and convolution integral are defined in the theoretical section. This study compares the flexible and conventional protocols, considering the differences in parameters based on simulations. Conclusions are drawn based on the parameter errata, deviations, and statistical tests given in the simulations. The study's outcome is that simulations based on a given blood curve support that the flexible series is more accurate for ptMBF than fixed ones. The simulation characteristic leads to limitations of conclusions, and for more reliable results, further study is required.

Keywords: Compartment model, Convolution integral, Laplace transform, Myocardial PET, Radiowater, Simulation, Time-activity curve

Tämä Pro Gradu -tutkielma käsittelee joustavia radiovesi PET-protokollia. Lokeromalli, josta keskeiset parametrit johdetaan, sekä matemaattiset käsitteet kuten Laplace -muunnos ja konvoluutiointegraali, määritellään teoriaosiossa. Tutkimus vertailee joustavia protokollia jo käytössä olleisiin hyödyntämällä simulaatioissa saatuja parametrien välisiä eroja. Johtopäätökset perustuvat virheisiin parametreissa, hajontoihin ja tilastolliseen testaukseen, simulaatioon pohjautuen. Tämän tutkimuksen lopputulos on että tiettyyn verikäyrään pohjautuvat simulaatiot tukevat väitettä että joustavat sarjat ovat tarkempia ptMBF suhteen kuin ennaltamääritellyt sarjat. Simulaatiopiirre johtaa päätelmien rajoittuneisuuteen ja luotettavammat tulokset vaativat jatkotutkimusta.

Avainsanat: Aika-aktiivisuuskäyrä, Konvoluutiointegraali, Laplace muunnos, Lokeromalli, Myokardiaalinen PET, Radiovesi, Simulaatio

Contents

1 Introduction **1**

2 Positron emission tomography (PET) **2**
2.1 Basics of myocardial PET 2
2.2 Main properties of ^{15}O-water 2
2.3 Radioactive decay of ^{15}O 3
2.4 Flexible vs fixed PET 3

3 Laplace transform **5**
3.1 Profounding analysis concepts 5
3.2 Laplace transform basics 6
3.3 Inverse Laplace transform 8
3.4 Convolution integral 9

4 Compartment model **11**
4.1 Deriving the tissue radioactivity concentration 11
4.2 Arterial blood volume parameter and perfusable tissue fraction 14

5 Methods **15**
5.1 Referenced frame series for simulations 15
5.2 Characteristics of flexible frame series 16
5.3 Computer software and application 16
5.3.1 Simulation software 16
5.3.2 Flexible frame series' generator application 17
5.4 Completing the simulations 18
5.5 Computing the errors 18
5.6 Statistical testing and the significance of differences 19

6 Results **20**
6.1 Time-activity curves and parameter values 20
6.2 Differences between the series illustrated and described 22

7 Discussion **25**
7.1 Frame lengths 25
7.2 Some alternatives for possible further study 25

8 Conclusions **27**

References **28**

Appendices **31**

1 Introduction

This thesis compares fixed and flexible frame series for myocardial positron emission tomography (myocardial PET). Fixed series does not change between imaging procedures, but flexible series are practically different each time.

There are three parameters: perfusable tissue myocardial blood flow, perfusable tissue fraction, and arterial volume. The interest is to see if there are positive differences in perfusable tissue myocardial blood flow, ptMBF, for flexible series compared to fixed series. The interest is, too, if these differences are significant. Also, deviations of parameter values are studied because they affect the quality of an image. The region of interest, ROI, is the area based on which the parameters are computed.

The main research question is whether a PET procedure with flexible frame lengths gives more desirable values for selected parameters than a procedure with fixed frame lengths and no flexibility in frame timings. The word flexible refers to a frame series where each frame has an equal number of counts, or decay events, as possible after the maximum radioactivity on ROI is achieved.

This study considers whether the error in the parameters with frames fixed in advance differs compared to having a flexible series with three different minimum lengths of frames.

There is more weight on perfusable tissue myocardial blood flow (ptMBF) parameters compared to perfusable tissue fraction (PTF) and arterial volume (VA) parameters. The simulation values for each frame series are given for all three of them. Then, the differences in parameter locations between series are statistically tested using a two-sided Wilcoxon test. The difference between each pair of series is significant if there is a p-value less than 0.05, denoted as $p < 0.05$.

For flexible frame length series, three different minimum lengths of frames are considered: 5 s, 3 s, and 2 s. The last one mentioned may be relatively short for technology when writing this study, but the first two should be applicable at some level. Furthermore, the longest minimal frame length, 5 s, has generally been used on series having fixed frames during this study.

This study first presents basics of positron emission tomography in Section 2. Mathematical results are given in Section 3 and the model the theory is based is presented in Section 4. Then Section 5 describes the methods of this study. Section 6 presents results this study concludes. Finally Section 7 discusses this study and the results and Section 8 draws the conclusions.

2 Positron emission tomography (PET)

Positron emission tomography, abbreviated as PET, is a medical imaging procedure that applies radioactive tracers. It is a part of nuclear medicine. PET has been in use for multiple decades and is involved, for example, in oncologic, cardiac, and neurological imaging [18]. Positron emission tomography is an efficient "non-invasive" method to study, for example, myocardial functionality [15]. Being often non-invasive, PET has made it an effective procedure in contrast to invasive ones.

In the 21st century, PET combined with computed tomography, PET-CT has been widely applied because it combines anatomical and metabolic imaging [12]. PET-CT technique is hence commonly used in medical imaging. The technical aspects in the field of PET are continuously developing, and there is also more advanced technique, such as magnetic resonance imaging combined with positron emission tomography, MRI-PET, and more.

In clinical use, the patient is set in the scanner tube and injected with a radiotracer. The scanner collects information about radioactivity, and then the image is constructed with an algorithm-based process that applies theoretic models [28]. The development of those algorithms is an ongoing process. Image accuracy has been improving over time.

2.1 Basics of myocardial PET

PET imaging is a valuable tool for cardiac diagnostics. The procedure gives crucial data regarding symptoms of possible coronary artery disease [10]. PET imaging offers access to information that other methods can have difficulty providing.

In [10], the tracer was 2-(fluorine-18) fluoro-2-deoxy-g-glucose, or FDG, that had been in standard use before the 21st century. However, the science of nuclear medicine is developing continuously, including tracers.

2.2 Main properties of ^{15}O-water

Radiowater,^{15} O-water, is now much more prevalent in clinical use than in the very beginning of the 21st century [7]. Radiowater's usage has been growing in the diagnostics of coronary artery disease. It has many beneficial properties for myocardial PET [7].

A water molecule has two hydrogen atoms and one oxygen atom. An oxygen atom usually has 16 electrons, but in ^{15}O-water, also called radiowater, the oxygen has only 15 electrons. The missing electron makes the molecule radioactive; ^{15}O is a radionuclide with a half-life near 2 minutes [17].

In the Radiowater molecule, the oxygen nuclides decay to nitrogen and positron. PET scanners recognize these positrons; this forms the basis for the image construction.

2.3 Radioactive decay of ^{15}O

The formulas and half-life appear on the websites of Turku PET Centre [20] and National Nuclear Data Center [19], respectively. The half-life of oxygen-15 is 122.24 s. Radioactivity at a given point in time can be solved using a formula where A_0 is the radioactivity at $t = 0$:

$$A_t = A_0 e^{-\lambda t}. \tag{1}$$

The decay constant λ is crucial in computations. The following formula gives the half-life of the isotope.

Definition 1. (Decay constant) The decay constant is based on a formula below where $T_{1/2}$ is the half-life of the isotope

$$\lambda = \frac{\ln 2}{T_{1/2}}.$$

The radioactivity at a given moment can be computed using Equation 1 in general case. For radiowater there is the result Lemma 2 gives.

Lemma 2 (Radioactivity at given time)**.** *Given the half-life of oxygen*-15 *is* 122.24 s*,*

$$\lambda = \frac{\ln 2}{122.24}.$$

then radioactivity at the moment t *in seconds is*

$$A_t = A_0 e^{-\frac{\ln 2}{122.24} t}.$$

We need to know when x % radioactivity is left compared to $t = 0$. It can be computed using Corollary 3. The radioactivity at the moment t is given by Equation 2.

Corollary 3. *Time there is* x*% radioactive counts compared to maximum density. There is*

$$A_t = A_0 e^{-\frac{\ln 2}{122.24} t}.$$

Solving this for t *gives*

$$t = -\frac{122.24 \ln \frac{A_t}{A_0}}{\ln 2}. \tag{2}$$

2.4 Flexible vs fixed PET

Traditional PET has predetermined frame lengths, while flexible protocol sets each frame's lengths during the PET imaging procedure. While using a flexible process, the frames can be determined based on the list-mode data of a PET camera.[23] Follows that we can access the total number of counts at a given time.

We are now studying partially flexible PET procedures where the beginning of the procedure behaves like conventional protocol. Still, after the maximum density of counts is reached, the protocol is based on radioactive decay of ^{15}O. This study

applies the idea of flexibility by finding the point with the highest density of radioactive counts, and the behavior of frame times is predetermined before and after this point in time.

It is likely that, in some cases, flexible property could be applied more thoroughly. However, this thesis aims to show how flexible protocol could be used in myocardial PET and compare its efficacy to existing series in a specific case.

3 Laplace transform

Laplace transform has an input function that is time-domained and gives an output function that is frequency-domained with complex values, as Schiff states in his book [24]. This transform is beneficial if the goal is to find a function of frequency when given a function of time. The first subsection provides the mathematical grounds for building the theory of Laplace transform and then convolution integral.

Basic ideas on Laplace transforms in the Subsection 3.2 give a base for results needed to justify the model. The inverse Laplace transform, discussed in Subsection 3.3, explains the model for parameters. It is often used in solving differential equations besides convolution integral and gives a function of time when the input is a function of frequency.

The convolution integral is a more advanced concept based on the theory of Laplace transform. It is general while solving differential equations. The idea of convolution integral is presented in Subsection 3.4.

This section is mainly based on Schiff's book [24] unless there is another reference for some results.

3.1 Profounding analysis concepts

The concepts of piecewise continuity and absolute convergence of an integral are required to justify the Laplace transform. In this study, the set of real numbers is denoted by $\mathbb{R}$.

The function must be piecewise continuous, as in Definition 4, because for the Laplace transform, the integral must be defined on every interval $[0, b)$, for any $b \in \mathbb{R}$.

Definition 4 (Piecewise continuous function.)**.** A function f is piecewise continuous in a non-negative range $[0,\ \infty)$ if it fulfils the following two properties:
1) There exists $\lim_{t\to 0^+} f(t)$, and
2) The function is continuous on every finite interval $(0,\ b),\ b \in \mathbb{R}$, but can have jump discontinuities on some individual points.

The Laplace transform also requires that the integral converges absolutely; that is, the integral has a finite limit while $\lim_{b\to\infty} f(b)$.

The following Definitions 5, 6 and 7 for improper integral, the convergence of integral, and its absolute convergence, respectively, are based on Harjulehto et al. book [6].

Definition 5 (Improper integral)**.** Let $f : [0,\ \infty)$ be integrable on every interval $[0,\ c] \subset [0,\ b)$. Then the improper integral is the function $E(x) : [0,\ \infty) \to \mathbb{R}$ defined:

$$E(x) = \int_0^x f(y)\ dy.$$

Now that there is defined the the improper integral in Definition 5. For Definition 7 of the absolutely converging integral, the more general definition of the converging improper integral as Definition 6 is required.

Definition 6 (Convergence of improper integral)**.** If $E(x) : [0,\ \infty) \to \mathbb{R}$ is an improper integral as in Definition 5 and $\lim_{x\to\infty} E(x) = r$, such that $r \in \mathbb{R}$ then the improper integral converges. The value of converging improper integral is r.

Definition 7, the absolute convergence of integral, is applied in justifying that a Laplace transform exists.

Definition 7 (Absolutely convergent integral.)**.** Assume the function $f : [0,\ b) \to \mathbb{R}$ is integrable on every interval $[0,\ c] \subset [0,\ b)$. If the improper integral

$$\int_0^b |f(x)|dx$$

converges, then the integral

$$\int_0^b f(x)dx$$

converges absolutely.

3.2 Laplace transform basics

The Laplace transform presented in Definition 8 transforms a function of time to a function of frequency. In this thesis, it is used as a part of the solution process for an ordinary differential equation while justifying the parameters. The definition for Laplace transform below is based on the reference [24].

Definition 8 (Laplace transform)**.** Let $f(t)$ be a function assuming $t \geq 0$ and the domain being time. Then the Laplace transform $\mathscr{L}$ of function $f(t)$ is

$$\mathscr{L}\{f(t)\} = \int_0^\infty f(t)e^{-st}\ dt \tag{3}$$

$$= \lim_{t\to\infty} \int_0^t f(t)e^{-st}\ dt. \tag{4}$$

The following Example 9 illustrates how to apply Definition 8 for an exponential function.

Example 9 (Applying Laplace transform)**.** Find the Laplace transform of $f(t) = e^t$, while $0 \leq t < \infty$.

Solution. To find $\mathscr{L}(e^t)$, the function should be plugged into integral Formula 4 given by the Laplace transform Definition 3, and is then solved, as follows:

$$\begin{aligned}\mathscr{L}(e^t) &= \int_0^\infty e^t e^{-st} dt \\ &= \int_0^\infty e^{t(1-s)} dt \\ &= \frac{e^{t(1-s)}}{1-s} + C.\end{aligned}$$

The Laplace transform of the given function $f(t)$ is then $\mathscr{L}(e^t) = \frac{e^{t(1-s)}}{1-s} + C$.

The preceding example is relevant to the parameters considered later because it includes an exponential function, which is usual for physical science applications. The Definition 10 of exponential order is needed as an assumption to show the transformation $\mathscr{L}f(t)$ exists.

Definition 10 (Exponential order)**.** . A function f has a exponential order α if there are for some $t_0 \leq 0$ non-negative and finite real constants M and α such that,

$$|f(t)| < Me^{\alpha t}, \ while \ t \leq t_0.$$

If there is an assumption that $s \in \mathbb{R}$, it can be stated that the Theorem 11 justifies the existence of a Laplace transform.

Theorem 11 (Existence of Laplace transform)**.** *If the function f is piecewise continuous (Definition 4) in the range $[0, \ \infty)$, and is of exponential order α, see Definition 10, then the Laplace transform $\mathscr{L}(f(t))$ exists for $s > \alpha$.*

Proof. Because f is of exponential order α then there is a finite $M_1 > 0$ such that,

$$|f(t)| \leq M_1 e^{\alpha t}, \quad t \leq t_0.$$

The function f is also piecewise continuous, that will say it has a supremum on $[0, \ t_0)$, that can be written as $M_2 e^{\alpha t}$, where M_2 is finite and non-negative, hence

$$|f(t)| \leq M_2 e^{\alpha t}, \quad 0 < t < t_0.$$

Because any exponential function $e^{\alpha t}$ gets only positive values on the range $[0, \ t_0]$, by using a constant $M = \max\{M_1, M_2\}$ it is possible to combine the previous two inequalities to,

$$|f(t)| \leq Me^{\alpha t}, \quad t > 0.$$

Now that there is an upper bound for $|f(t)|$, the Laplace transform is rewritten:

$$\int_0^T |e^{-st} f(t)| dt \leq M \int_0^T e^{(\alpha - s)t} dt.$$

Computing the integral gives:

$$= \frac{M}{s-\alpha} - \frac{Me^{-(\alpha-s)T}}{s-\alpha}.$$

Letting $T \to \infty$ and remembering that $s > \alpha$, because f is of exponential order α. Then there is

$$\int_0^\infty |e^{-st} f(t)| dt \leq \frac{M}{s-a}.$$

Follows that the Laplace integral converges absolutely while $s > \alpha$. □

The previous Theorem 11 gives information on whether there exists a Laplace transform. The following Theorem 12 will show that an existing Laplace transform preserves linearity. This property is applied in solving equations for parameters later on.

Theorem 12 (Linearity of Laplace transform)**.** *Let f_1 and f_2 be linear functions of exponential order α_1 and α_2 respectively. Assume $c_1,\ c_2 \in \mathbb{R}$. Then $c_1 f_1(t) + c_2 f_2(t)$ is linear and of exponential order $\alpha = \max \alpha_1,\ \alpha_2$, and there is*

$$\mathscr{L}(c_1 f_1 + c_2 f_2) = c_1 \mathscr{L}(f_1) + c_2 \mathscr{L}(f_2).$$

Proof. The proof is based on the integral's property to preserve the linearity. There is given a justification in Schiff's book [24] on pages 16-17. □

The previous knowledge is applied further in the following subchapter presenting the inverse Laplace transform that can make computations in both directions using the Laplace transform.

3.3 Inverse Laplace transform

The theorems presented in this subsection are based on Schiff's book [24].

The inverse Laplace transform can be applied in solving differential equations and is presented in Definition 13.

Definition 13 (Inverse Laplace transform)**.** Assume there is a Laplace transform $\mathscr{L}(f(t)) = F(s)$ then the corresponding inverse Laplace transform is

$$\mathscr{L}^{-1}(F(s)) = f(t).$$

The uniqueness of a Laplace inverse transform is required in many physics applications and later on, while solving a differential equation. Theorem 14, Lerch's theorem, is given in Schiff's book [24], without proof.

Theorem 14 (Distinct continuous functions on a non-negative range have distinct Laplace transforms)**.** *Assume function $f(t)$ is continuous on $[0,\ \infty)$, then the inverse Laplace transform*

$$\mathscr{L}^{-1}(F(s)) = f(t),$$

is uniquely defined.

The uniqueness of Laplace transforms can be assumed in this study because there is a positive range, and the functions in differential equations are continuous.

3.4 Convolution integral

The convolution is a concept required in many physics applications. In this study, it is used to show how to derive the most central parameters from models. First there is presented Definition 15, that gives grounds for convolution,

Definition 15 (Convolution integral)**.** Assume $f(t)$ and $g(t)$ are piecewise continuous functions on $[0,\ \infty)$, then the convolution integral is defined as

$$(f * g)(t) = \int_0^t f(t)g(t-\tau)d\tau.$$

Theorem 16 for the product of two convolution integrals is crucial while solving equations on parameters related to the model. It states that while having two piecewise continuous functions of exponential order, the Laplace transform of their convolution can be written as a product of two distinct Laplace transforms.

Theorem 16 (Convolution theorem)**.** *Assume f and g are piecewise continuous functions on $[0,\ \infty)$, and they are of exponential order α. Then,*

$$\mathscr{L}[(f * g)(t)] = \mathscr{L}(f(r))\mathscr{L}(g(s)),\ s > \alpha$$

Proof. Begin with

$$\mathscr{L}(F(s)\mathscr{L}(g(s)) = \int_0^\infty f(\tau)e^{-st}d\tau \int_0^\infty e^{-su}g(u)du$$

because the integrals do not have common integrating factors, there is

$$\mathscr{L}(f(s))\mathscr{L}(g(s)) = \int_0^\infty f(\tau)e^{-s\tau} \int_0^\infty g(u)e^{-su}du\ d\tau.$$

Now, by properties of integral by an exponential function

$$\mathscr{L}(f(s))\mathscr{L}(g(s)) = \int_0^\infty f(\tau) \int_0^\infty g(u)e^{-s(\tau+u)}du\ d\tau.$$

Next substituting $u = t - \tau$ leads to

$$\mathscr{L}(f(s))\mathscr{L}(g(s)) = \int_0^\infty f(\tau) \int_\tau^\infty g(t-\tau)e^{-st}dt\ d\tau.$$

Reversing the integration

$$\mathscr{L}(f(s))\mathscr{L}(g(s)) = \int_0^\infty \left(\int_0^t f(\tau)g(t-\tau)e^{-st}d\tau \right) dt.$$

Rearranging the exponential term

$$\mathscr{L}(f(s))\mathscr{L}(g(s)) = \int_0^\infty \left(\int_0^t f(\tau)g(u-\tau)d\tau \right) e^{-s\tau}dt.$$

The Definition 15 referring to convolution gives

$$\mathscr{L}(f(s))\mathscr{L}(g(s)) = \int_0^\infty \left(\int_0^t f(\tau)g(u-\tau)d\tau \right) e^{-s\tau} dt.$$

The result

$$\mathscr{L}[(f * g)(t)] = \mathscr{L}(f(s))\mathscr{L}(g(s)),$$

follows. □

Now, the mathematical definitions and theorems that the justification of parameters for the compartment model requires are presented. However, a general model describing the dynamic system is given before justifying the crucial parameters.

4 Compartment model

This study applies a one-tissue compartment model or, say, a two-compartment model. Figure 1 illustrates the model describing the radioactivity on myocardial area ^{15}O-PET. Here, there is considered such a model that has the artery tracer concentration in one compartment and the region of interest radioactivity $D_m(t)$ in another compartment.

There are two transition constants. The first describes the transition from the artery area to the region of interest (ROI); this is written formally using extraction fraction E, blood flow f, and tissue fraction α as $K_1 = EF\alpha$. For simplicity, there can be written $K_1 = f = EF\alpha$. The second transition coefficient k_2 considers the flow away from the ROI. That is formulated by using, in addition to the components in K_1, the tissue/blood partition coefficient p. The coefficient k_2 is then written $k_2 = f/p$.

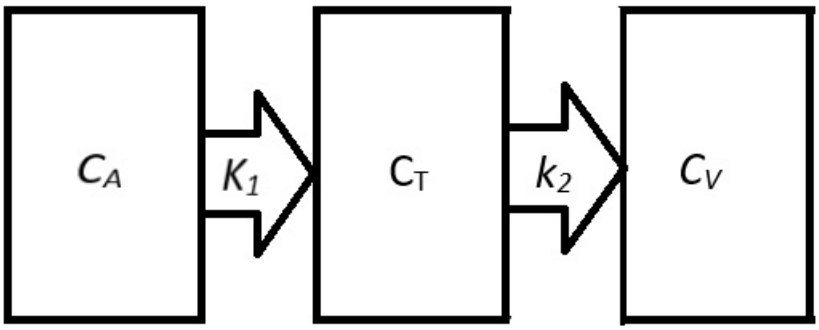

Figure 1: The one-tissue model with parameters $K_1 = f$, and $k_2 = \frac{f}{p}$ to apply for myocardial ^{15}O-PET.

4.1 Deriving the tissue radioactivity concentration

This subsection discusses large parts of Iida et al. article [8], which shows how to derive computations for myocardial blood flow parameter, abbreviated MBF. Derivation is done by varying the principle of inert gas exchange by Kety and Schmidt (1945), [13]. The tissue fraction given in Definition 17 is the considerable difference between the myocardial blood flow and the traditional gas exchange model. The tissue fraction is the tissue mass divided by the region's volume of interest.

Definition 17 (Tissue fraction)**.** Let W be the tissue mass in $d[g]$, and V the volume of ROI (Region of interest) in $[ml]$, then the tissue fraction α is defined

$$\alpha = \frac{W}{V}$$

and its unit is $[g/ml]$.

Let E be the extraction fraction, F the blood flow $[ml/min]$, p the tissue/blood partition coefficient in ml/g, $C_A(t)$ the tracer artery concentration in $\mu Ci/ml$, and $C_T(t)$, the net tissue concentration in μCi and C_V the concentration in the capillary and venous blood in $\mu Ci/ml$.

According to the Iida et al. study, the following first-order ordinary differential equation represents the tracer balance $\frac{dC(t)}{dt}$, as Definition 18 states.

Definition 18 (The tracer balance in the region of interest (ROI))**.** The differential equation can express the tracer balance in the region of interest:

$$\frac{dC_T(t)}{dt} = K_1 C_A(t) - k_2 C_T(t)$$

, while $C_A(t)$ refers to the tracer artery concentration and C_T to the net tissue tracer concentration.

The net tissue concentration is impossible to detect but can be solved using $D_m(t)$, measured ROI concentration. Definition 19 gives a formula for the net tissue concentration.

Definition 19 (The net tissue concentration formula)**.** The net tissue concentration $C_T(t)$ can be written in terms of the measured ROI concentration $D_m(t)$ using the tissue fraction.

$$D_m(t) = \alpha C_T(t)$$

Theorem 20 (The derivative of measured ROI concentration)**.** *The derivative of the measured ROI concentration $D_m(t)$ equals to the difference of tracer artery C_A and tracer tissue C_T concentrations weighted by K_1 and k_2, describing the speed of the flow,*

$$\frac{dD_m(t)}{dt} = \alpha K_1 C_A(t) - k_2 C_T(t).$$

Proof. Begin with

$$\frac{dC_T(t)}{dt} = K_1 C_A(t) - k_2 C_T(t).$$

Here C_T is the tracer net tissue concentration, and substituting $C_T = \frac{D_m(t)}{\alpha}$ to the left side of the equation gives

$$\frac{1}{\alpha}\frac{dD_m(t)}{dt} = K_1 C_A(t) - k_2 C_T(t).$$

multiplying the both sides by α gives

$$\frac{dD_m(t)}{dt} = \alpha K_1 C_A - k_2 \alpha C_T(t).$$

Substituting $D_m(t) = \alpha C_T$ results

$$\frac{dD_m(t)}{dt} = \alpha K_1 C_A - k_2 D_m(t).$$

□

In Theorem 21 there is proved a differential equation (Equation 5), that describes the concentration of radioactivity in the region of interest.

Theorem 21 (ROI formula)**.** *Concentration in the ROI at the time t is described by the function $C_T(t)$ when assuming the initial condition $C_T(0) = 0$.*

$$C_T(t) = \alpha K_1 C_A(t) * e^{-k_2/t}. \tag{5}$$

Proof. Theorem 20 gives

$$\frac{dC_T(t)}{dt} = K_1 C_A(t) - k_2 C_T(t).$$

Rewriting it as standard form first order linear ordinary differential equation (ODE)

$$C_T(t)\frac{d}{dt} + k_2 C_T(t) = K_1 C_A(t).$$

Finding the integrating factor

$$\mu = e^{\int k_2 dt},$$

that is

$$\mu = e^{k_2 t}.$$

The constant in integration can be omitted because the initial value at $t = 0$ equals 0. For this type of ODE, there is

$$C_T(t) = \frac{\int (\mu K_1 C_A(t))dt + C}{\mu}.$$

Substituting μ gives:

$$C_T(t) = \frac{\int e^{k_2 t} K_1 C_A(t)dt + C}{e^{k_2 t}}.$$

Then, arranging terms leads to

$$C_T(t) = \frac{K_1 \int e^{k_2 t} C_A(t)dt + C}{e^{k_2 t}}.$$

Replacing Laplace transform, see definition 8, gives

$$C_T(t) = \frac{K_1 \mathscr{L}\{-k_2 C_A\}[t] + C}{e^{k_2 t}}.$$

Rewriting $\frac{1}{e^{k_2 t}} = e^{-(k_2)t}$, gives

$$C_T(t) = K_1 \mathscr{L}\{-k_2 C_A\}[t] e^{-k_2 t} + C e^{-k_2 t}.$$

Applying the convolution theorem, see Theorem 16, leads to

$$C_T(t) = K_1 (C_A(t)) * e^{-k_2 t} + C e^{-k_2 t}.$$

Considering the initial condition and hence letting $C = 0$, the results

$$C_T(t) = K_1 (C_A(t)) * e^{-k_2 t}.$$

□

Remark 22 combines Theorem 21 to the idea of the tissue radioactivity concentration curve (TAC).

Remark 22. Now that we have solved the ODE for concentration in the region of interest $C_T(t)$, we have found the tissue radioactivity concentration curve:

$$D_m(t) = K_1 C_A(t) * e^{-k_2 t}.$$

4.2 Arterial blood volume parameter and perfusable tissue fraction

This subsection is based on Iida et al. article [9]. We can derive the arterial blood volume from the formula for measured radioactivity concentration for some region of interest (ROI). The goal is to solve the formulas for the arterial blood volume V_a.

A theorem for ROI radioactivity concentration C_T has already been proved; see Theorem 21. It is utilized while deriving the theorem for the left-ventricular concentration curve.

Definition 23 on left-ventricular time activity curve presents the curve as Equation 6.

Definition 23 (LV time-activity curve)**.** Denote the time-activity curve describing the radioactivity on a given left ventricular region as $C_{LV}(t)$. While β refers to recovery coefficient having values between 0.0 and 1.0, γ, there is the following equality:

$$C_{LV}(t) = \beta C_A(t) + (1 - \beta)C_T(t). \tag{6}$$

Definition 24 including the water perfusable tissue fraction concept, presents the Equation 7 that gives the measured radioactivity concentration at a given time.

Definition 24. For a given myocardial ROI having α denoting PTF - water-perfusable tissue fraction, and V_A the vascular volume fraction, the measured radioactivity concentration function $C_{ROI}(t)$ is:

$$C_{ROI}(t) = \alpha C_(t) + V_A C_A(t). \tag{7}$$

5 Methods

5.1 Referenced frame series for simulations

After searching and reviewing scientific articles, by groups of Aikawa [2], Danad [4], Germino [5], Kajander [11], Sciagrà [25] and Yoshinaga[27], considering myocardial PET with ^{15}O on adults, the frame series shown in table 5.1 were chosen to the simulations. Lubberink et al. [14] have applied the same series as Danad's group [4], and the same applies to Adachi et al. [1] and Kajader et al. [11]. Danad et al. and Kajander et al. seemed to be the original references; hence, they were chosen for this text.

This study compares their parameter differences and the flexible protocol represented later in this thesis. Some series resemble each other; they were taken to the study to increase the scope because there were few procedures to study.

For series with total length longer than 300 s, there were extrapolation issues with the simulation software that was in use; therefore, these are shortened so that their maximal length is 300 s, and the changes are as minor as possible. It isn't easy to evaluate for certainty if the results would have been different with another type of simulation program, and that is why the results in this study are only directional.

In the latter sections, some assumptions based on these series results are not likely to get significantly better on the scope of this study if there were all frames in simulation. These assumptions are based on mathematical analysis principles and a general idea of connecting the series with flexible frames and mathematics concepts.

Frame length	Aikawa, et al. [2]	Danad, et al. [4]	Germino, et al. [5]	Kajander, et al. [11]	Sciagrà et al. [25]	Yoshinaga, et al. [27]
10s		x1			x1	
3s			x20			
5s		x8		x14	x8	x6
10s	x18	x4	x10	x3	x4	
15s		x2			x2	x6
20s		x3	x6	x3	x3	
30s	x4(6)	x2		x4	x2	x6(8)
60s		x1(2)				
Total length	300 (360)	300 (360)	280	280	240	300 (360)

Table 2: Referenced frame series for this study.

5.2 Characteristics of flexible frame series

The goal is to create three flexible frame series with varying technological demands to compare with the ones in use around 2020. The first flexible series is well applicable considering technology 2023. The second is theoretically functional, with more developed technology in use at the moment of the study. The third series is probably optimal in 2023 but presents the potential of a flexible-type series. The main criteria for creating a new flexible frame series has been that each frame should contain an equal number of counts as possible. That makes the pictures as comparable quality as possible. Figure 5.2 describes the process of creating flexible series.

While trying to reach an equal radioactive count number, it is clear that soon after the radiotracer injection, the counts' density is very high compared to the latter phase of the scan. That is why the frames before the maximum of time activity curve (TAC) are set to be of a constant length: 5, 3, or 2 s, depending on each series's minimum frame length.

Depending on the series, a 2, 3, or 5 s length frame is centered around the maximum TAC. Then, frames before the maximum are placed backward until there is a negligible number of counts in a frame. There is a negligible number of counts practically before the injection is given.

After the frame is centered to the maximum of TAC, the number of counts in each frame has been tried to be set to be equal to the frame following the centered one as possible. The Equation 2 from Corollary 3 is applied in these computations. Alternatively, one can think there is an idea of TAC's integral role behind these computations.

As a concise description, there are constant length frames until the maximum TAC is reached. Then, the length of each frame is computed in whole seconds based on having as equal of many counts as possible as the first frame after the one centered around the maximum of TAC.

5.3 Computer software and application

Software is a crucial part of this study. The successive simulations were a prerequisite for all the reasoning. Presenting the results in the scope of the study was only possible with functional and reliable simulation software. In addition to simulation software, a simple frame file generator was executed for creating flexible series' frame files. The code for frame file generator is on Appendix 1.

5.3.1 Simulation software

The simulations are completed using a TPCCLIB library and simulation software [22] developed by Vesa Oikonen at Turku PET centre. The blood curve this study applies stems from Oikonen's TPCCLIB package [22].

It was possible to run two different frame series at a time with software. A run

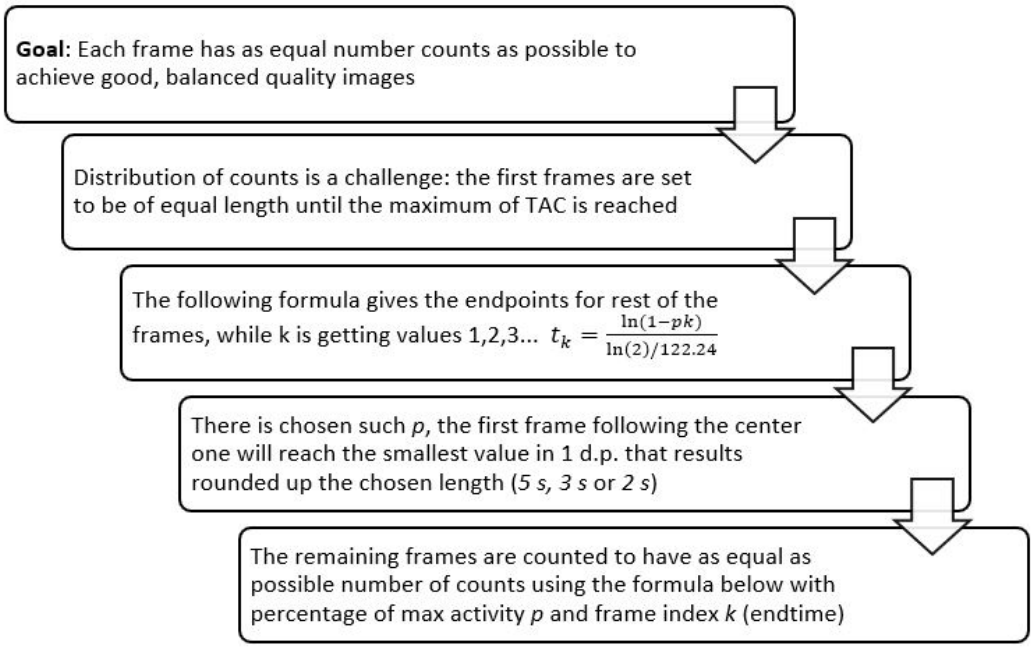

Figure 3: Description of the process for creating flexible series.

resulted in folders for the series $sim1$ and $sim2$ and a folder with additional files used in the simulation. The parameter values are available on these folders separately on .res files or as assembled on the fitted_parameters.html file.

5.3.2 Flexible frame series' generator application

Manual creation of many frame files based on a percentage of radioactive decay was found to be laborious using Excel only. Thus, I wrote a Python application that returns a frame document in .txt -format. The application computes the frames-based radioactive decay and adds the top section with file information. Finally, after getting the text files, I converted the files manually to correct .sif -format.

The application takes the degradation percentage, the point of time with maximum radiation density, and the number of frames after maximum radiation as input parameters besides the minimal frame length. After the application creates the file, the format is manually changed to .sif and renamed as desired. The simulation software used required files named 'frame1.sif' and 'frame2.sif'.

In the application, there is computed

$$t_k = \frac{\ln(1-pk)}{\ln(2)/122.24}$$

where p is the percentage of counts in each frame after the centered frame, and k is the index - $k = 1$ for the first frame after TAC maximum. The final start time for frame k is t_k rounded to the nearest integer.

5.4 Completing the simulations

The simulation software was run for each frame set, two sets simultaneously using .sif files, see Appendix 1. The results were collected from the folders, including the fitted_parameters and .res files. The errors for parameters were first calculated using a spreadsheet, but fitted_parameters.html files gave the tabulated values and are illustrative. Therefore, the final decision was to take the values from tables from .html files to show the values for the central parameters and some vital statistics, such as mean and standard deviation. Some of the parameters in HTML files are excluded because they are not within the scope of this study.

The following parameters Oikonen represents at the Turku PET Centre modeling website are in the scope of this study: perfusable tissue blood flow (ptMBF), arterial blood volume (VA), and perfusable tissue fraction (PTF) [21]. The parameter of primary interest in this study is ptMBF, and Va and PTF are of secondary interest. Hence, error in ptMBF is to be minimized while it is checked. There is not much greater error for Va or PTF than for references.

The result tables are gathered from the HTML files the simulation software creates. After that, the mean root square error and mean absolute errors are computed for each series and parameter. Finally, statistical testing was run for differences between locations of the ptMBF variable for different series.

5.5 Computing the errors

Two different formulas for error are used to illustrate and clarify the differences between series more profoundly. Both of these are described in the article by Chai and Draxler [3]. The first formula is root mean square error, and the second is mean absolute error.

Root mean square error has the general formula $\sqrt{\frac{\sum_{i=0}^{n}(x-x_i)^2}{n+1}}$. According to article [3], the variance of the sample affects the root mean square more than the mean absolute error, which does not weigh any values more than others. The formula in this case, where the sample size is 6, is:

$$RMSE = \sqrt{\frac{\sum_{i=0}^{5}(x-x_i)^2}{6}}$$

where x is respectively 1.00 for ptMBF, 0.60 for PTF and 0.25 for Va, and x_i are the parameter values moved $0, 1, ...4$ or 5 s.

The formula for mean absolute error is $\frac{\sum_{0}^{n}\sqrt{(x-x_i)^2}}{n+1}$. Previously presented root mean square error has been popular and widely used in modeling. Still, because variance has no special weight in it and each value has the entirety of the same weighting, its features differ from RMSE. The formula for MAE we use is:

$$MAE = \frac{\sum_{0}^{5}\sqrt{(x-x_i)^2}}{6}.$$

5.6 Statistical testing and the significance of differences

A two-sided pairwise Wilcoxon's test is applied for each pair of data sets. The test is described thoroughly by its founders, Mann and Whitney, in a journal article [16]. Hence, this test can also be called the Mann-Whitney U-test.

Tests were completed for the ptMBF parameter because it has been chosen to be the most central aspect of this study. For each flexible series found during this study, the statistical significance was tested for differences in ptMBF parameter location in both directions compared to the series we referenced. A p-value of 0.05 has been used as a measure of significance.

6 Results

These results presented are purely based on a blood curve by TPCCLIB software [22], Vesa Oikonen, and applying results further in the preclinical study requires a greater amount and diverse data.

6.1 Time-activity curves and parameter values

There are tables with results for parameter values for each series. For 2 *s* series, see Table 4

Minimum 2 s frames flexible series

Study	ptMBF	PTF	Va
0s	0.9999	0.5999	0.2499
1s	1.0003	0.5999	0.2500
2s	1.0002	0.5998	0.2500
3s	1.0002	0.5998	0.2500
4s	1.0001	0.5998	0.2500
5s	1.0001	0.5998	0.2500
Min	0.9999	0.5998	0.2499
Max	1.0003	0.5999	0.2500
Median	1.0002	0.5998	0.2500
Mean	1.0001	0.5998	0.2500
SD	0.0001	0.0001	0.0000

Table 4: Simulated parameter values for a flexible series with minimum 2 *s* frames

For series with 3 *s* minimum frame length, see Table 5.

Germino et al. Series

Study	ptMBF	PTF	Va
0s	1.0027	0.5995	0.2499
1s	1.003	0.5995	0.2499
2s	1.0029	0.5994	0.25
3s	1.003	0.5994	0.2499
4s	1.0033	0.5994	0.2499
5s	1.0032	0.5993	0.25
Min	1.0027	0.5993	0.2499
Max	1.0033	0.5995	0.25
Median	1.003	0.5994	0.2499
Mean	1.003	0.5994	0.2499
SD	0.0002	8E-05	5E-05

Minimum 3 s frames flexible series

Study	ptMBF	PTF	Va
0s	1.001	0.5998	0.2499
1s	1.0016	0.5998	0.25
2s	1.0014	0.5997	0.25
3s	1.0014	0.5997	0.25
4s	1.0015	0.5998	0.25
5s	1.0013	0.5997	0.2501
Min	1.001	0.5997	0.2499
Max	1.0016	0.5998	0.2501
Median	1.0014	0.5998	0.25
Mean	1.0014	0.5998	0.25
SD	0.0002	6E-05	6E-05

Table 5: Simulated parameter values for series with minimum 3 *s* frames.

Table 6 presents the simulated parameter values for series with minimum frame length at least 5 s.

Aikawa et al. 2 last frames removed

Study	ptMBF	PTF	Va
0s	1.0206	0.5997	0.2491
1s	1.0174	0.5992	0.2496
2s	1.0149	0.5986	0.2502
3s	1.0134	0.5982	0.2508
4s	1.0125	0.5981	0.2511
5s	1.0125	0.5982	0.2510
Min	1.0125	0.5981	0.2491
Max	1.0206	0.5997	0.2511
Median	1.0142	0.5984	0.2505
Mean	1.0152	0.5987	0.2503
SD	0.0032	0.0007	0.0008

Danad et al. - last frame removed

Study	ptMBF	PTF	Va
0s	0.9923	0.6003	0.2456
1s	0.9937	0.6000	0.2461
2s	0.9964	0.5997	0.2470
3s	0.9999	0.5993	0.2480
4s	1.0030	0.5991	0.2487
5s	1.0051	0.5987	0.2493
Min	0.9923	0.5987	0.2456
Max	1.0051	0.6003	0.2493
Median	0.9982	0.5995	0.2475
Mean	0.9984	0.5995	0.2475
SD	0.0051	0.0006	0.0015

Kajander et al.

Study	ptMBF	PTF	Va
0s	1.0056	0.5997	0.2498
1s	1.0051	0.5995	0.2499
2s	1.0049	0.5995	0.2500
3s	1.0052	0.5996	0.2499
4s	1.0056	0.5996	0.2498
5s	1.0058	0.5996	0.2498
Min	1.0049	0.5995	0.2498
Max	1.0058	0.5997	0.2500
Median	1.0054	0.5996	0.2499
Mean	1.0054	0.5996	0.2499
SD	0.0004	0.0001	0.0001

Sciagrá / clinical: Aarhus, Uppsala...

Study	ptMBF	PTF	Va
0s	0.9935	0.6000	0.2456
1s	0.9949	0.5997	0.2460
2s	0.9974	0.5994	0.2469
3s	1.0009	0.5991	0.2479
4s	1.0039	0.5988	0.2487
5s	1.0060	0.5985	0.2493
Min	0.9935	0.5985	0.2456
Max	1.0060	0.6000	0.2493
Median	0.9992	0.5993	0.2474
Mean	0.9994	0.5993	0.2474
SD	0.0050	0.0006	0.0015

Yoshinaga et al. - 2 last frames removed

Study	ptMBF	PTF	Va
0s	0.9812	0.5913	0.2527
1s	0.9759	0.5906	0.2531
2s	0.9705	0.5900	0.2535
3s	0.9653	0.5896	0.2537
4s	0.9601	0.5892	0.2538
5s	0.9543	0.5888	0.2539
Min	0.9543	0.5888	0.2527
Max	0.9812	0.5913	0.2539
Median	0.9679	0.5898	0.2536
Mean	0.9679	0.5899	0.2535
SD	0.0100	0.0009	0.0005

Minimum 5 s frames flexible series

Study	ptMBF	PTF	Va
0s	1.0020	0.5997	0.2493
1s	1.0034	0.5997	0.2495
2s	1.0042	0.5996	0.2497
3s	1.0041	0.5993	0.2500
4s	1.0040	0.5993	0.2501
5s	1.0042	0.5993	0.2501
Min	1.0020	0.5993	0.2493
Max	1.0042	0.5997	0.2501
Median	1.0041	0.5995	0.2499
Mean	1.0037	0.5995	0.2498
SD	0.0009	0.0002	0.0003

Table 6: Simulated parameter values for series with minimum 5 s frames or longer.

The first six represented in Table 6 are comparable in the sense they have a minimum frame length of 5 s or longer in the case of upper left cornered series by Aikawa et al., namely 10 s.

Germino et al. and the flexible series in Table 5 have the minimum frame length of 3 s. The parameter values seem much more optimal than in Table 6. The deviations for these two series seem quite the same, but they are minimal, and there can be relative differences. However, the flexible one seems to give a lot, about a half, less error than the series by Germino's group.

The minimum length of a frame 2 s is a bit optimal at the time of this study, but Table 4 shows how the parameters get better values when frames are shortened.

Time activity curves are presented in Appendix 3.

6.2 Differences between the series illustrated and described

Figure 7 illustrates the deviation in myocardial blood flow parameter values moved 0 to 5 s for all the series. (* The last frame was removed for technical reasons, ** The last two frames were removed for technical reasons).

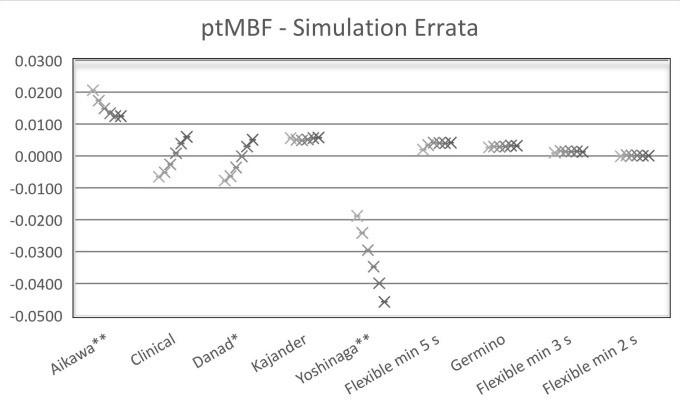

Figure 7: Errata in ptMBF, * last frame removed, ** 2 last frames removed for technical limitations.

The deviations and values illustrated in Figure 7 strengthen the idea that for series with longer frames, the Kajander et al. study and flexible series seem to be the most reliable. The same applies to Germino and flexible series with middle-length frames; the latter one seems better in terms of ptMBF.

The illustration for perfusable tissue fraction PTF, Figure 8, resembles somewhat the results for ptMBF, but the errata are smaller.

For arterial volume parameter, there is more deviation for some series, as the

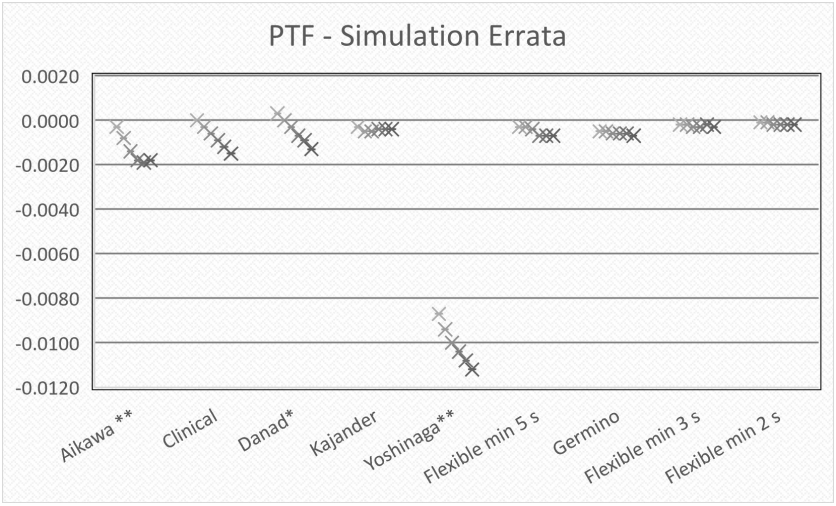

Figure 8: Errata in PTF, * last frame removed ** 2 last frames removed for technical reasons.

illustration in Figure 9 presents. However, still Kajander's and Germino's group has got reliable-looking results in this simulation, as well as the three flexible series.

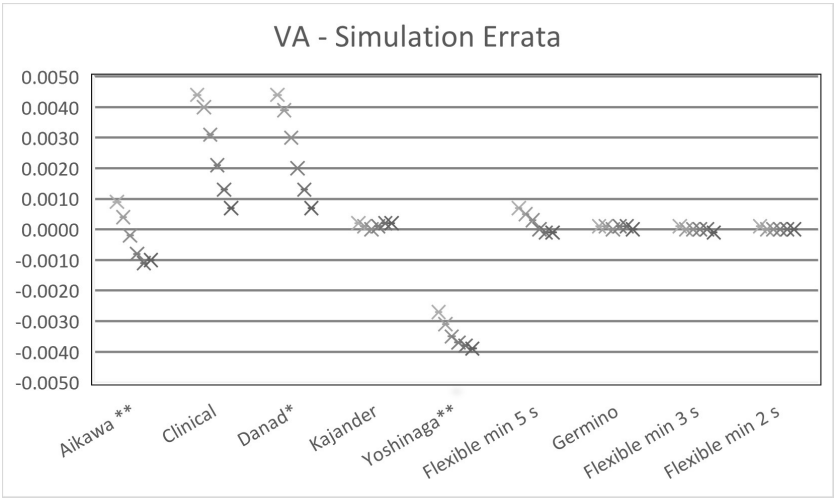

Figure 9: A graph illustrating errata in VA, * last frame removed, ** 2 last frames removed because of technical limitations.

Table 10 gives Wilcoxon's U-test's p-values between the flexible and referenced series. The 5 s series has no significant difference from the Germino et al. series, but Germino et al. have a minimum frame length of 3 s instead of 5 s. These results seem promising. The clinical series and Danad et al. have more standard deviation in ptMBF than flexible 5 s, no matter whether their mean/median is relatively near the reference value. The ptMBF is this study's main interest, and the statistical test's values seem reasonable. Or PTF, between Danad's group serie and 5 s flexible,

p values, U-test	2 s flexible			3 s flexible			5 s flexible		
	ptMBF	PTF	VA	ptMBF	PTF	VA	ptMBF	PTF	VA
Aikawa, et al.	0.0355*	0.0355*	0.3441	0.0313*	0.0355*	0.3441	0.0313*	0.0579	0.0938
Clinical (Upsala...)	0.8438	0.0625	0.0313*	0.4375	0.0936	0.0313*	0.0938	0.2807	0.0313*
Danad, et al.	0.4375	0.2476	0.0313*	0.2188	0.4185	0.0313*	0.0585	1.0000	0.0313*
Germino, et al.	0.0350*	0.0263*	0.1489	0.0313*	0.0305*	0.0719	0.1148	0.2695	0.4004
Kajander, et al.	0.0355*	0.0310*	0.0568	0.0313*	0.0335*	0.0579	0.0355*	0.2718	0.5248
Yoshinaga, et al.	0.0313*	0.0313*	0.0313*	0.0313*	0.0313*	0.0355*	0.0313*	0.0313*	0.0313*

Table 10: Statistical significance for parameter differences between the reference and flexible series.

there may have been equal values, and hence, the test appears unlikely to work as wanted.

7 Discussion

The flexible series developed in this study seems effective and reliable considering the simulations committed by using the TPCCLIB library. For ptMBF and PTF, the simulation results for flexible series are better than most references in this study. The VA parameter for flexible 5 *s* series could be better, but many referenced series gave even more distribution and errata in simulations.

The statistical tests resulted in significant differences for some parameters and series, but only a few. The results after this simulation study are promising, but further conclusions can only be drawn after additional studies with more data and resources are completed.

The simulations have limitations, and this study has limitations. The results are limited because there is no real-life experiment, only a computer simulation. Furthermore, there is no variety in the scope of this study because there is only one blood curve in use.

7.1 Frame lengths

An interesting outcome of this study is that the results are getting more accurate while increasing the frequency of the frames, at least for the method in flexible series.

It might be possible to get better results, say, compared to the 3 *s* series, if the tenths of the seconds in the frame lengths are allowed.

This study assumes there are whole seconds in frame lengths, but the first frame with negligible counts is not considered in this case. This assumption makes the procedure technically efficient. However, advances in technology and computing software may enable different types of lengths.

7.2 Some alternatives for possible further study

The first step could be to study simulations with another blood curve data. Only one blood curve was available for the simulation input during this study. If the results follow a similar pattern with different input data, one can make stronger assumptions about the functionality of flexible series.

The next step after this study is more simulations with different blood curve data or research with a mechanical heart-emulating device. If this supports the results of this study, then animal imaging experiments would be needed before possible clinical experiments if the preclinical study gives safe and promising results.

The changes between the existing referenced series and 5 *s* series would seem small, but because the medical imaging field, accuracy and safety must always be studied carefully in multiple phases.

In the case of this blood curve, using a flexible procedure instead of a fixed one,

more accurate parameter values are achieved for ptMBF. However, it is impossible to evaluate how these different types of frame series behave for each blood curve and even more impossible to predict at the time of this study if there is a chance for clinical use one day. Hence, further analysis is required for flexible PET protocols.

8 Conclusions

Based on the simulation results, there might be potential for flexible myocardial PET of this type. Any strong arguments or conclusions for the functionality of flexible series cannot be made for certainty because of the type of this study.

The simulation characteristic and having only one blood curve are the main reasons this study provides a limited view of the case. However, it showed some potential with the resources available compared to the referenced series. Hence, further analysis can give more evidence to support the optimality of the series found in this study.

References

[1] Adachi, I., Gaemperli, O., Valenta I., Schepsis, T., Siegrist, P., Treyer, V., Burger, C., Morita, K., & Kaufmann, P. (2007). Assessment of myocardial perfusion by dynamic O-15–labeled water PET imaging: Validation of a new fast factor analysis. Journal of Nuclear Cardiology, 14(5), 698–705. https://doi.org/10.1016/j.nuclcard.2007.05.012

[2] Aikawa T., Naya M., Obara M., Manabe O., Magota K., Koyanagawa K., Asakawa N. Ito Y. M., Shiga T., Katoh C., Anzai T., Tsutsui H., Murthy V. L. & Tamaki N.(2019) Effects of coronary revascularization on global coronary flow reserve in stable coronary artery disease, Cardiovascular Research, 115(11)10, 119–129, https://doi.org/10.1093/cvr/cvy169

[3] Chai, T. C., & Draxler, R. R. (2014). Root mean square error (RMSE) or mean absolute error (MAE)? – Arguments against avoiding RMSE in the literature. Geoscientific Model Development, 7(3), 1247–1250. https://doi.org/10.5194/gmd-7-1247-2014

[4] Danad I, Raijmakers P. G., Appelman Y.E. , Harms H.J. , de Haan S & van den Oever M. L. (2013) Hybrid imaging using quantitative H215O PET and CT-based coronary angiography for the detection of coronary artery disease. J Nucl Med. (54), 55–63. https://doi.org/10.2967/jnumed.112.104687

[5] Germino, M., Ropchan, J., Mulnix, T., Fontaine, K., Nabulsi, N., Ackah, E., Feringa, H., Sinusas, A. J., Liu, C., & Carson, R. E. (2016a). Quantification of myocardial blood flow with 82Rb: Validation with 15O-water using time-of-flight and point-spread-function modeling. EJNMMI Research, 6(1). https://doi.org/10.1186/s13550-016-0215-6

[6] Harjulehto, P., Klén, R., & Koskenoja, M. (2014). Analyysiä reaaliluvuilla (1st ed.). Unigrafia Oy, Helsinki.

[7] Harms, H. J., Huisman, M. C., Knaapen, P., Lammertsma, A. A., & Lubberink, M. (2011, December). Parametric imaging of myocardial blood flow and viability using [15O]H2O and PET/CT. Imaging in Medicine, 3(6), 711–724. https://doi.org/10.2217/iim.11.58

[8] Iida, H., Kanno, I., Takahashi, A., Miura, S., Murakami, M., Takahashi, K., Ono, Y., Shishido, F., Inugami, A., & Tomura, N. (1988). Measurement of absolute myocardial blood flow with H215O and dynamic positron-emission tomography. Strategy for quantification in relation to the partial-volume effect. Circulation, 78(1), 104–115. https://doi.org/10.1161/01.cir.78.1.104

[9] Iida, H., Rhodes, C. G., de Silva, R., Araujo, L. I., Bloomfield, P. M., Lammertsma, A. A & Jones, T. (1992). Use of the Left Ventricular Time-Activity Curve as a Noninvasive Input Function in Dynamic Oxygen-15-Water Positron Emission Tomography. Journal of Nuclear Medicine. https://jnm.snmjournals.org/content/33/9/1669.long

[10] Jadvar, H., Strauss, H. W., & Segall, G. M. (1999, July). SPECT and PET in the Evaluation of Coronary Artery Disease. RadioGraphics, 19(4), 915–926. https://doi.org/10.1148/radiographics.19.4.g99jl08915

[11] Kajander S, Joutsiniemi E, Saraste M, Pietilä M, Ukkonen H, Saraste A, et al. Cardiac positron emission tomography / computed tomography imaging accurately detects anatomically and functionally significant coronary artery disease. Circulation. 2010;122:603–13. https://doi.org/10.1161/CIRCULATIONAHA.109.915009.

[12] Kapoor, V., McCook, B. M., & Torok, F. S. (2004, March). An Introduction to PET-CT Imaging. RadioGraphics, 24(2), 523–543. https://doi.org/10.1148/rg.242025724

[13] Kety, S. S., & Schmidt, C. F. (1945). The Determination of Cerebral Blood Flow in Man by the Use of Nitrous Oxide in Low Concentrations. American Journal of Physiology, 143(1), 53–66. https://doi.org/10.1152/ajplegacy.1945.143.1.53

[14] Lubberink, M., Harms, H. J., Halbmeijer, R., de Haan, S., Knaapen, P., & Lammertsma, A. A. (2010). Low-Dose Quantitative Myocardial Blood Flow Imaging Using 15O-Water and PET Without Attenuation Correction. Journal of Nuclear Medicine, 51(4), 575–580. https://doi.org/10.2967/jnumed.109.070748

[15] Medical Advisory Secretariat.(2010). Positron emission tomography for the assessment of myocardial viability: an evidence-based analysis. Ontario health technology assessment series, 10(16), 1–80.

[16] Mann, H. B.,& Whitney, D. R. (1947). On a Test of Whether one of Two Random Variables is Stochastically Larger than the Other. Annals of Mathematical Statistics, 18(1), 50–60. https://doi.org/10.1214/aoms/1177730491

[17] National Center for Biotechnology Information. (2022). PubChem Compound Summary for CID 10129877, Water O-15. Retrieved September 25, 2022 from https://pubchem.ncbi.nlm.nih.gov/compound/Water-O-15.

[18] NHS. (2021, November 18). PET scan. Nhs.uk. Retrieved September 24, 2022, from https://www.nhs.uk/conditions/pet-scan/

[19] National Nuclear Data Center (n.d.). NuDat 3. Retrieved October 15, 2023 from https://www.nndc.bnl.gov/nudat3/

[20] Oikonen, V., Tolvanen, T.(2022). Decay correction. http://www.turkupetcentre.net/petanalysis/decay.html

[21] Oikonen, V. (2021). TPC - Long time frames in myocardial radiowater analysis. http://www.turkupetcentre.net/petanalysis/frames_mbf.html

[22] Oikonen, V. (2022). TPCCLIB v. 0.7.8 [Computer software]. University of Turku. Retrieved March 16, 2023 https://gitlab.utu.fi/vesoik/tpcclib.

[23] Rahmim, A., Tang, J. and Zaidi, H. (2009), Four-dimensional (4D) image reconstruction strategies in dynamic PET: Beyond conventional independent frame reconstruction. Med. Phys., 36: 3654-3670. https://doi-org.ezproxy.utu.fi/10.1118/1.3160108

[24] Schiff, J. D. (1999). The Laplace Transform: Theory and Applications. Springer.

[25] Sciagrà, R., Lubberink, M., Hyafil, F., Saraste, A., Slart, R. H. J. A., Agostini, D., Nappi, C., Georgoulias, P., Bucerius, J., Rischpler, C., & Verberne, H. J. (2020). EANM procedural guidelines for PET/CT quantitative myocardial perfusion imaging. European Journal of Nuclear Medicine and Molecular Imaging, 48(4), 1040–1069. https://doi.org/10.1007/s00259-020-05046-9

[26] Thiagarajan, S. (2022, August). Theory of Laplace Transforms and Their Applications. Retrieved November 29, 2022, from https://math.uchicago.edu/ may/REU2022/REUPapers/Thiagarajan.pdf.

[27] Yoshinaga, K., Klein, R., Kasai, K., Tomiyama, Y., Manabe, O., Naya, M., Sakakibara, M., Tsutsui, H., deKemp, R. A., & Tamaki, N. (2012). Quantification of regional myocardial blood flow estimation with three-dimensional dynamic rubidium-82 PET and modified spillover correction model. Journal of Nuclear Cardiology, 19(4), 763–774. https://doi.org/10.1007/s12350-012-9558-1

[28] Zioga, M. (2012, December 1). Image Reconstruction in the Positron Emission Tomography|HNPS Advances in Nuclear Physics. Retrieved September 24, 2022, from https://eproceedings.epublishing.ekt.gr/index.php/hnps/article/view/2490

Appendix 1: Code for frame files application

```
import numpy as np
import time as fortime
import datetime


def framecount (start, cent, dfnumber, minl, filename):


    # Initializes the starting values:

    starting=str(start)
    div=round(start % 1, 1)
    stime=int(start-div)
    dfnr = dfnumber
    frames = []


    # Creates a table for integer values rounded down up to turning point and finds its size

    while stime>7:
        stime=stime-minl
        frames.append(int(stime))
    frameslen=len(frames)


    # Initializes the constants for decay

    constant = np.log(2)/(122.24)
    maxi = 1
    concentration = 1
    k = 1
    prev = starting


    # Computes and writes times for frames after the turning point

    decayframes = []
    for k in range (1,dfnr):
        time0 = np.log(1-cent*k)
        time = -time0/constant
        time2 = str(int(time)+start)
        if k <= dfnr:
            decayframes.append(time2)
```

```
# Writes the header:

nroffframesstr = str(dfnr + frameslen)
number1str = str(1)
number2str = str(2)
ctime = datetime.datetime.now()
dateandtime= ctime.strftime("%d/%m/%Y %H:%M:%S")
with open (filename, 'w') as f:
        f.writelines( dateandtime + ' ' + nroffframesstr + ' ' + number2str + ' ' + number1str
                    + ' ' + 'FRA1' + '\n')


# Writes the 1-decimal float-values for points of time to the txt-document

with open (filename, 'a') as f:
    f.writelines(str(0.0) + ' ' + str(frames[len(frames)-1]+div) + '\n')
leng = len(frames)
while leng>1:
    leng=leng-1
    framefrom=str(frames[leng]+div)
    frameto=str(frames[leng-1]+div)
    with open (filename, 'a') as f:
        f.writelines(framefrom + ' ' + frameto + '\n')
with open (filename, 'a') as f:
        f.writelines(str(frames[0]+div)+ ' ' + str(starting) + '\n')

# Writes the decay frames

with open (filename, 'a') as f:
            f.writelines(starting + ' ' + decayframes[0] + '\n')
for co in range (1, dfnr-2):
        with open (filename, 'a') as f:
            f.writelines(decayframes[co-1] + ' ' + decayframes[co] + '\n')
with open (filename, 'a') as f:
            f.writelines(decayframes[dfnr-3] + ' ' + decayframes[dfnr-2])
```

Appendix 2: Figures for flexible frame series files with .sif format

The 5 s flexible series

```
15/02/2023 21:00:24 32 2 1 FRA1 O-15
0.0 6.9
6.9 11.9
11.9 16.9
16.9 21.9
21.9 26.9
26.9 31.9
31.9 36.9
36.9 41.9
41.9 47.9
47.9 53.9
53.9 59.9
59.9 65.9
65.9 72.9
72.9 78.9
78.9 85.9
85.9 93.9
93.9 100.9
100.9 108.9
108.9 117.9
117.9 125.9
125.9 134.9
134.9 144.9
144.9 154.9
154.9 165.9
165.9 177.9
177.9 189.9
189.9 203.9
203.9 217.9
217.9 233.9
233.9 250.9
250.9 269.9
269.9 291.9
```

The 3 s flexible series

```
15/02/2023 21:11:24 53 2 1 FRA1 O-15
0.0 5.9
5.9 8.9
8.9 11.9
11.9 14.9
14.9 17.9
17.9 20.9
20.9 23.9
23.9 26.9
26.9 29.9
29.9 32.9
32.9 35.9
35.9 38.9
38.9 42.9
42.9 45.9
45.9 49.9
49.9 52.9
52.9 56.9
56.9 60.9
60.9 64.9
64.9 67.9
67.9 71.9
71.9 75.9
75.9 80.9
80.9 84.9
84.9 88.9
88.9 93.9
93.9 97.9
97.9 102.9
102.9 107.9
107.9 112.9
112.9 117.9
117.9 122.9
122.9 128.9
128.9 133.9
133.9 139.9
139.9 145.9
145.9 152.9
152.9 158.9
158.9 165.9
165.9 172.9
172.9 179.9
179.9 186.9
186.9 194.9
194.9 203.9
203.9 211.9
211.9 220.9
220.9 230.9
230.9 240.9
240.9 251.9
251.9 263.9
263.9 275.9
275.9 288.9
288.9 302.9
```

The 2 s flexible series

```
14/02/2023 19:14:33 75 2 1 FRA1 O-15
0.0 6.4
6.4 8.4
8.4 10.4
10.4 12.4
12.4 14.4
14.4 16.4
16.4 18.4
18.4 20.4
20.4 22.4
22.4 24.4
24.4 26.4
26.4 28.4
28.4 30.4
30.4 33.4
33.4 35.4
35.4 37.4
37.4 40.4
40.4 42.4
42.4 44.4
44.4 47.4
47.4 49.4
49.4 52.4
52.4 54.4
54.4 57.4
57.4 60.4
60.4 62.4
62.4 65.4
65.4 68.4
68.4 71.4
71.4 74.4
74.4 76.4
76.4 79.4
79.4 82.4
82.4 85.4
85.4 89.4
89.4 92.4
92.4 95.4
95.4 98.4
98.4 102.4
102.4 105.4
105.4 108.4
108.4 112.4
112.4 116.4
116.4 119.4
119.4 123.4
123.4 127.4
127.4 131.4
131.4 135.4
135.4 139.4
139.4 143.4
143.4 147.4
147.4 152.4
152.4 156.4
156.4 161.4
161.4 166.4
166.4 171.4
171.4 176.4
176.4 181.4
181.4 186.4
186.4 192.4
192.4 198.4
198.4 204.4
204.4 210.4
210.4 216.4
216.4 223.4
223.4 229.4
229.4 237.4
237.4 244.4
244.4 252.4
252.4 260.4
260.4 268.4
268.4 277.4
277.4 287.4
287.4 296.4
296.4 307.4
```

Appendix 3: Time activity curves

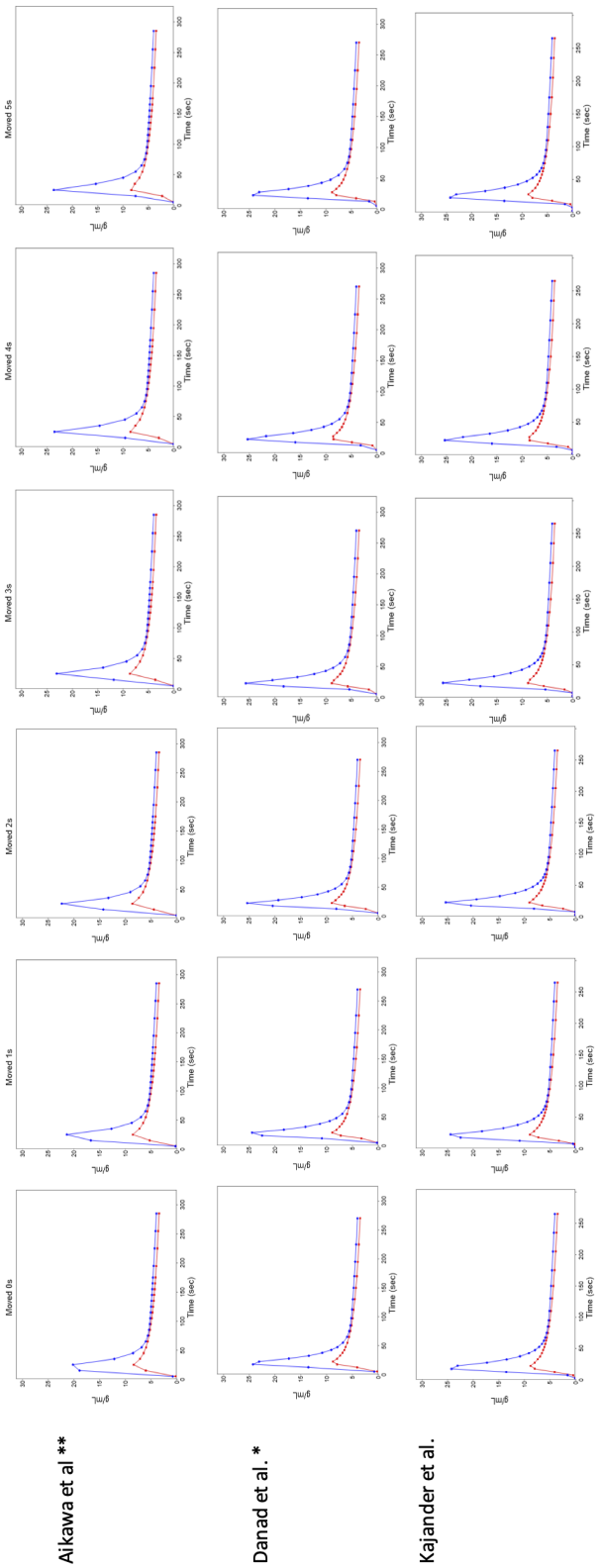

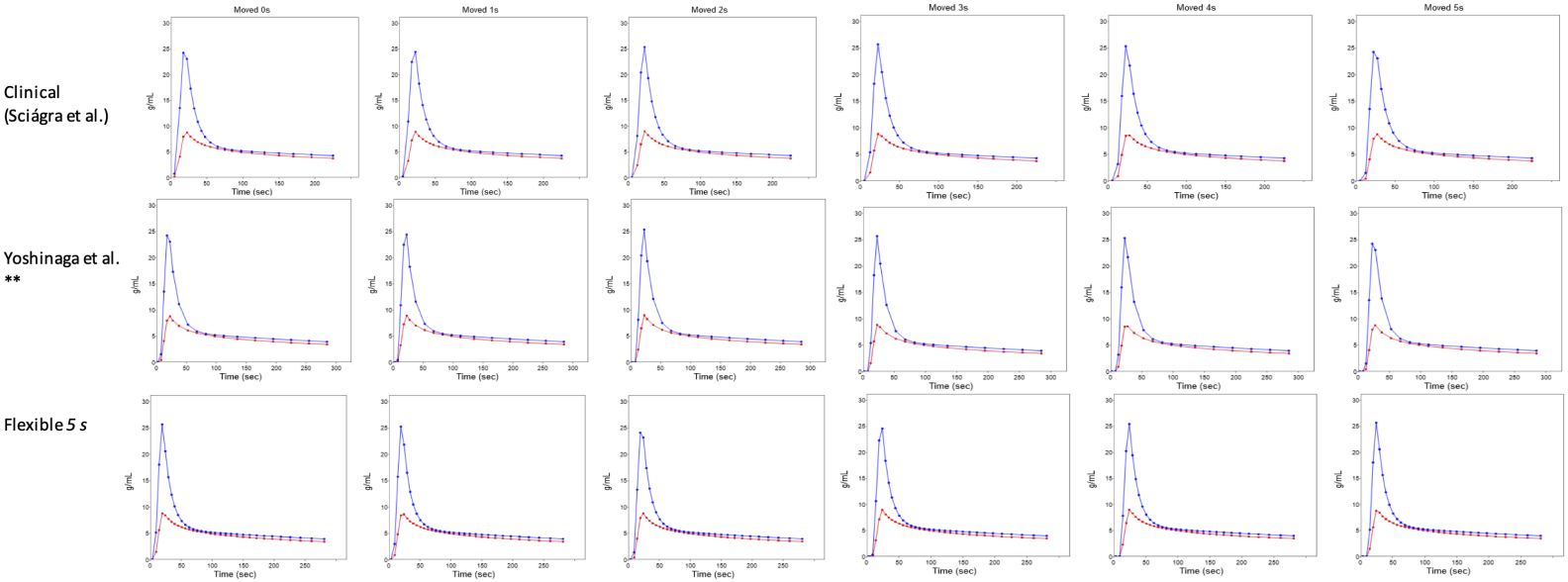

Clinical (Sciágra et al.)

Yoshinaga et al. **

Flexible *5 s*

Germino et al.

Flexible *3 s*

Flexible *2 s*